# Performance of OMPS Nadir Profilers' Sensor Data Records

C. Pan[a], B. Yan[b], C. Cao [b], L. Flynn[b], X. Xiong[c], E. Beach[d] and L. Zhou[b]
[a]ESSIC, University of Maryland, College Park, MD 20740; [b] NOAA STAR, College Park, MD 20746; [c]SSAI, Lanham, MD 20706; [c]ERT, Laurel, MD 20707; and [d]I. M. Systems Group Inc., Rockville, MD 20852

***Abstract*— The Ozone Mapping and Profiler Suite (OMPS) Nadir Profilers (NPs) are advanced backscatter ultraviolet (BUV) hyperspectral instruments that measure ozone profiles in the Earth atmosphere. The first NP sensor onboard the Suomi National Polar-orbiting Partnership (Suomi NPP) satellite began its science observations on 26 January 2012 after its aperture door opened. The second OMPS NP, flying on the NOAA-20 satellite, was launched on November 18, 2017. The two NP sensors acquire Earth spectral images along their satellite flight path with a 16.7° wide swath, enabling weekly coverage of vertical ozone distribution in the Earth atmosphere. A successful thorough sensor calibration enables the NP sensors' data records (SDRs) to meet measurement accuracy requirements. This paper provides SDRs accuracy analysis for both NP sensors, and discusses important aspects of the SDRs performance in relation to the sensors' characterization and calibration.**

***Index Terms*— SNPP, JPSS, OMPS, radiometric calibration, charge coupled device (CCD), remote sensing, and sensor data record (SDR), radiometric, stray light, wavelength**

## I. Introduction

The Suomi NPP Ozone Mapping and Profiler Suite (OMPS) Nadir Profiler (NP) and the NOAA-20 OMPS NP are two of a series of ozone monitoring sensors flown by NOAA and NASA. Both NP sensors have a spectral coverage over 250 nm to 310 nm with each spectral pixel encompassing an approximate sampling resolution of ~0.42 nm. However, the Suomi NPP NP has a total of 147 wavelength channels and the NOAA-20 NP has 151 wavelength channels. The NP sensors measure backscatter ultraviolet radiation at the top of the Earth atmosphere, providing information to retrieve Earth atmospheric ozone concentrations in specified layers of a vertical column on a global scale [1, 2 and 3]. Data records provided by the NP sensors extend the nearly 40-year ozone data records created by predecessors such as the Backscatter Ultraviolet (BUV) onboard the Nimbus-4 satellite [4 and 5]. Similar to the second Backscatter Ultraviolet (SBUV/2) instrument, each NP sensor is a double grating spectrometer that measures nadir-profiling radiances via its two-dimensional CCD detectors. Algorithms used by the NPs in the SBUV/2 are adopted to create SDRs and ozone environment data records (EDRs) in both the Suomi NPP and NOAA-20 NPs. Table 1 provides the allocated SDR algorithm performance requirements and the corresponding NP sensors' properties. The expected Signal-to-Noise ratios (SNRs) in Table 2 are higher than those attained by the SBUV/2 sensors. Additionally, each NP equips with a depolarizer inside its telescope system to minimize the incoming linear polarization sensitivity during on-orbit operation.

## II. Sensor Data Records (SDRs)

The two NP sensors create Earth view SDRs that are time referenced, Earth geo-located, and radiance calibrated. The Suomi-NPP NP CCD array pixel measurements are binned into Raw Data Records (RDRs) on its spacecraft to create single macro-spatial pixels (93 spatial pixels are combined) by 147 spectral pixels (no spectral binning). The CCD array counts are aggregated over a total of 38 seconds creating data with a spatial resolution of 250 km x 250 km. The NOAA-20 NP CCD array measurements are binned into RDRs to create five macro-spatial pixels (19 spatial pixels are combined) by 151 spectral pixels (no spectral binning). Therefore, array counts are accumulated over a total of 7.6 seconds creating data with a higher spatial resolution of 50 km x 50 km. The one macro-spatial pixel and five macro-spatial pixels represent the spatial information contained within a total 16.7° of view in the cross-track direction.

OMPS flight software corrects sensor raw signals for non-linearity and relative pixel response, known as non-uniformity, when each NP sensor is making a science measurement. The flight software also bins CCD pixels to create macro-pixels in the spatial dimension. Calibrations for electronic bias, dark

TABLE 1
Algorithm Allocations and Sensor Properties

| Sensor Parameter | Baseline Algorithm Needs | Baseline Sensor Allocation | Note |
|---|---|---|---|
| Wavelength range | 252-306 nm | 250-310 nm | Ozone profiling |
| Bandwidth (FWHM) | 1.1 nm | 1.0 nm | Pair/triplet approach |
| Spectral sampling | 3.0 pixel/FWHM | 2.4 pixel/FWHM | λ shift, Ring effect |

| | | | |
|---|---|---|---|
| Number of channels | 8 discrete channels 252-306 nm | Hyperspectral coverage: 250-310 nm | Triplets, over-sampling, aerosols |
| Horizontal cell size | 250 km @ nadir | 250 km @ nadir | Heritage spatial sampling |
| SNR | From SBUV/2 spec | From SBUV/2 spec values | Precision |
| Polarization sensitivity | <5% | <5% | Accuracy |
| λ registration | < 0.01 nm | < 0.01 nm | Ozone cross section error |
| Albedo calibration | 2% | 2% | Accuracy |
| Pixel to pixel calibration (includes linearity) | 1% max. | 1% max. | Accuracy |
| Stray light | 1% | 1% | Accuracy and stability |

* The eight profiling wavelengths used in the retrieval algorithm are 251.97, 273.55, 283.08, 287.64, 292.27, 297.55, 301.93, and 305.80 nm.

TABLE 2
Signal-to-Noise Ratio Requirement

| Wavelength (nm) | Suomi-NPP NP 250 km x 250 km | NOAA-20 NP 50 km x 50 km |
|---|---|---|
| 250 - 273.6 | 35 | 7 |
| 273.6 - 283.1 | 100 | 20 |
| 283.1 -287.7 | 200 | 40 |
| 287.7-292 | 260 | 52 |
| 292-310 | 400 | 80 |

current, smear signal, and stray light signals take place during data ground processing. By applying sensor ancillary calibration information to the raw science data, the SDR algorithm converts raw sensor data into calibrated SDRs[6]. The ancillary information includes radiometric, spectrometric and geometric calibration coefficients and geo-referencing parameters like satellite platform ephemeris. As such, each NP's SDRs contain all major calibration coefficients and factors, and ancillary information needed to convert raw sensor counts to the calibrated Earth view radiance. The latter corrects for the sensor response change.

## III. SDR PERFORMANCE

A NP sensor registers signals detected spectrally and spatially through a two-dimensional CCD focal plane array mounted inside the sensor house. Theoretically, the number of countsfrom a NP CCD pixel detected at wavelength λ and integration time Δt can be expressed as [6]:

$$C_{ij}(\Delta t) = C_{ij}^{0}(\Delta t) + qe_{\lambda}\, p_{ij}\, r_{\lambda}\, g_e g_n L_{\lambda} \cos\theta_{ij}\, \Omega_p\, \Delta t \quad (1).$$

$$C_{ij}^{0}(\Delta t) = SL(\Delta t) + D(\Delta t) + W(\Delta t) + B \quad (2).$$

Practically, $C_{ij}^{0}(\Delta t)$ is a sum of stray light signals $SL(\Delta t)$, dark current $D(\Delta t)$, smear counts $W(\Delta t)$ and electrical bias $B$. Terms of gain, non-linearity, quantum efficiency, and Pixel Response Non-Uniformity (PRNU) do not enter the equation explicitly. Table 3 lists symbols and definitions of Eq.1 parameters. The mMeasured Earth radiance in a single pixel *(i, j)* can be written as a function of the corrected instrument counts,

$$Cij{:}L_{ij}(t) = C_{ij}(t)\, k_{ij}/\tau_{ij}(t), \quad (3)$$

where $L_{ij}$ is the derived Earth radiance; $K_{ij}$ is radiance coefficients that converts a count quantity to a radiance quantity; $\tau_{ij}(t)$ accounts for pixel response changes. The measured solar irradiance $Q_{ij}$ in the pixel *(i, j)* can be written as:

$$Q_{ij}(t) = C_{ij}^{s}(t)\, k_{ij}^{s}/g\rho(t)\tau_{ij}(t). \quad (4)$$

TABLE 3
Symbols and definitions of Eq. 1

| Quantity | Description |
|---|---|
| $qe_{\lambda}$ | Average quantum efficiency of the CCD at a wavelength |
| $p_{ij}$ | Photo-response non-uniformity for the pixel *(i,j)* |
| $r_{\lambda}$ | Response of the optical system |
| $Ge$ | The average gain of the entire image sensor and signal processing electronics system |
| $g_n$ | Nonlinearity of the gain signal processing electronics |
| $\theta_{ij}$ | Elevation angles of the observed point as viewed from *(i,j)* |
| $\Omega_p$ | Area-solid angle product of the instrument |
| $\Phi$ | Azimuth angles of the observed point as viewed from *(i,j)* |

Here, $C_{ij}^{s}$ is the irradiance mode counts; $k_{ij}^{s}$is the irradiance calibration coefficients; $\tau_{ij}$ accounts for the sensor throughput changes; $\rho$ is the solar diffuser plate reflectivity; $g$ is the relative angular irradiance response of the sensor. As such, an NP signal consists of a "real" term due to photons falling on the CCD as well as offset terms, such as dark current, stray light, smear and electrical bias as shown in Eq 2. These offsets must be subtracted during the RDR data processing prior to converting counts to radiances. Table 4 summarizes the major calibration terms associated with Eqs. 1- 4. These items are the key parameters to the SDR calibration and data accuracy. Following the prelaunch calibration methodology, we analyze the largest and averaged errors of the most of the calibration parameters within the range of scientific wavelengths for absolute radiance and irradiance calibration.

TABLE 4
SDR top level attributes and its corresponding sensor characterization

| Top-level requirement | System characterization |
|---|---|
| **Accuracy** | |
| Albedo calibration | Radiance |
| | Irradiance and goniometry |
| | Boresight (Pointing shifts and drifts) |
| Pixel-to-pixel radiometric calibration | Smear |
| | Dark current |
| | Linearity |
| | Pixel gain |
| | Goniometry (fine structure impact) |
| | Pixel response non-uniformity (PRNU) |
| | CCD system electronic bias |
| Wavelength calibration | Solar SNR |
| In-flight Wavelength shift | Goniometry errors |
| Intra-orbit wavelength stability | Spectral scale and band pass |
| Polarization | Polarization sensitivity |
| Stray light calibration | Point Spread Functions and OOB stray light |
| **Precision** | |
| Radiance SNR | Earth view measurement noise |
| Solar calibration SNR | solar measurement noise |
| Co-bore sighting | Spatial performance and boresight |

### *A. CCD Performance*

*1) Dark performance*

CCD dark signals are charges generated from thermal excitation of electrons into instrument conduction bands. Signals detected by CCD pixels accumulate in the CCD-wells even when there are no photons entering the device. Generation of dark electrons is a thermally activated process, and as such, the dark signals are strongly temperature dependent. Prelaunch test sets a doubling temperature of 7.0 ± 0.2°C (3- σ) control window. With a 3.7% dark size (the ratio of dark to signal), the dark calibration leads to an uncertainty of 0.07% in the absolute calibration, an insignificant error to the sensor measurements if the temperature is controlled tightly. In-flight operation cools the CCD focal plane to -45 ± 0.02 °C (3-σ) in control window. Therefore, temperature-introduced dark errors are greatly suppressed and are negligible in analysis. The dark calibration error from in-flight operation is mainly induced by a dark rate change (counts per second) over operation time. Fig 1 (a) shows changes of the in-flight dark rate in a time series for the Suomi-NPP NP (black) and NOAA-20 NP (gray). Trending of the dark current change starts on November 8, 2011 for the Suomi-NPP NP and on January 09, 2018 for the NOAA-20 NP. The change of the dark rate in the Suomi-NPP slows down about 65% after 8 years of operation [3]. The change in the NOAA-20 NP slowed down about 28% in the first three years since the launch: the weekly change dropped from 1.14% at launch to 0.8% at the current stage. There were two satellite maneuvers made for Suomi-NPP on day #961 and day #2250 that imposed temporal influences on the Suomi-NPP NP dark trend (appearing as two bumps in Fig.1 (a)), but the dark trend returned to the normal range afterwards.

Given the fact that the dark rate changes with time, an ideal calibration to remove the dark current in SDR calibration is a real time correction during a science data acquisition. Operationally, the frequency of the dark calibration is driven by the magnitude of the dark rate change, and the dark calibration is now on a weekly basis for both the NPs. Figure 1 (b) estimates the radiance error from the weekly dark calibration relative to a near real-time calibration for the Suomi-NPP NP (solid line) and the NOAA-20 NP (dashed line) at the current operational stage. As we expected, short wavelength channels have lower signal-to-noise ratios, thus resulting in relative larger errors. The maximum error of 0.53% for the Suomi-NPP NP and 0.34% for the NOAA-20 NP occurred at short wavelength 250 nm in the radiance calibration. However, the dark correction for solar irradiance calculation used near real time dark, so the calibration error is less than 0.01% for both NP sensors. Estimation of accuracy of albedo calibration over wavelengths found an average error of 0.05% for the Suomi-NPP NP and 0.03% for the NOAA-20 NP under the weekly dark calibration.

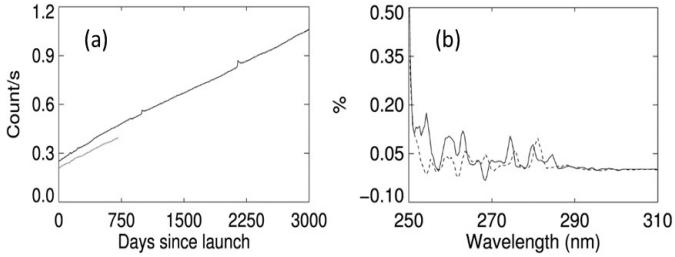


Fig. 1 a) Dark rate changes along mission time since the first in-flight dark measurement for the Suomi-NPP (black) and the NOAA-20 (gray). b) Calibration errors in Earth radiance retrieval from weekly calibration for the Suomi-NPP (solid) and the NOAA-20 (dashed).

*2) Smear signal*

Operated in a shutter-less system, the NP CCD readout signals contain smear components that originate from the incident signals on the CCD. The smear signal accumulates when the sensor transfers the image-frame from the photosensitive region into the storage region. To simplify the process of smear removal and gain correction, the NP sensor reads out 20 overclocked smear rows during an image transfer. The magnitude of the smear signal depends on a ratio of the transfer period to the total integration period and on the spatial content in the impinging image. For the NP sensor, the frame transfer time is 0.936 milliseconds, and 16 out of 20 smear rows are used for a smear correction gaining a factor of 4-times noise reduction. With in-flight electronic gain ($gain$) of 42.6 e–/count [3 and 7] and readout noise ($N_{readout}$) of 22.7 e–, the error of absolute radiance/irradiance calibration is about 0.015% calculated from Eq. 5,

$$E = \frac{Nreadout}{4gain}\frac{1.0}{C_{low}}, \quad (5)$$

where $C_{low}$ refers to a typical low signal (count) from in-flight Earth view measurements. Since error is a noise source, both radiance and irradiance calibrations have the same contribution to the albedo error, which is a sum of squares of the radiance errors, i.e., less than 0.03%.

The shorter imaging integration time and lesser spatial aggregation for the NOAA-20 NP compared to the Suomi-NPP NP created a greater sensitivity to transient spikes in the smear measurements used for the smear correction. These transient spikes usually add positive counts over a small number of pixels produced by the impact of a charged particle on the CCD. When a smear correction has been corrupted by such an event, the final corrected radiances will be lower than the true signal. For NOAA-20 NP, these can even produce negative radiances at higher solar zenith angles. The N20 algorithm implemented a smear filter in the SDR ground processing system to reduce the impact of the corrupted smear signals.

*3) Electronic bias*

The electronic offset bias of a CCD focal plane is a count level reading by amplifiers in absence of signals. The bias is set to a nonzero value to avoid underflow of negative current fluctuation due to CCD noise. We calculate the bias by averaging the center 8 of 12 trailing serial overclock pixels. This reduces the noise by a factor of square root of 8. Long term monitoring finds that the magnitudes of the bias are stable for both NP sensors: approximately741±1 counts over the past seven years for Suomi-NPP NP, and 672±1 counts for NOAA-20 NP. The total error contributes to the absolute radiance and irradiance calibrations is about 0.025% for Suomi-NPP NP and 0.028% for the NOAA-20 NP respectively. The combined error from radiance and irradiance calibration is about 0.04% for both NPs.

*4) Stray Light*

Stray light is a significant error source to the NP sensor measurements. The stray light comes from internal light scattering within the sensor that reaches the CCD detectors. Due to a finite size of the entrance pupil of the instrument, a light source directed to one pixel spreads out over adjacent pixels spectrally and spatially. Light from more than 2.5-nm away of the band center is classified as stray light as opposed to part of the band pass. This adds an unwanted contribution to the sensor signals. According to the prelaunch stray light calibration, less than a ~5% stray light was contributed to signals with an overall uncertainty of 0.02% in calibrations. In the in-flight sensor stray light analysis, we used a point spread functions (PSFs) model to predict the stray light signals by convolving a 2-D spectral image with the PSFs and derived stray light correction matrix. Calibration of stray light requires an accuracy of 1.0% on a global average level. Correlation analysis for the Suomi-NPP NP confirmed that the calibration met the requirement [8 and 9]. For the NOAA-20 NP, we collected more than 4800 measured radiance spectral images from various viewing conditions in order to evaluate the stray light correction on a global scale. Fig. 2 (a) demonstrates the global averaged stray light contribution in Earth view radiance is about 0.5 – 7.5% depending on wavelengths. The two gray lines represent boundaries of variations caused by different viewing conditions. It was estimated that less than 0.75% global error in the absolute radiance/irradiance calibration, and less than 0.38% error in the albedo calibration over all wavelengths for both NP sensors, as shown in Fig 2 (b) Thus, the stray light correction for the NOAA-20 NP meets the requirement. Furthermore, the stray light contribution partially cancels in a ratio of radiance to irradiance calculation.

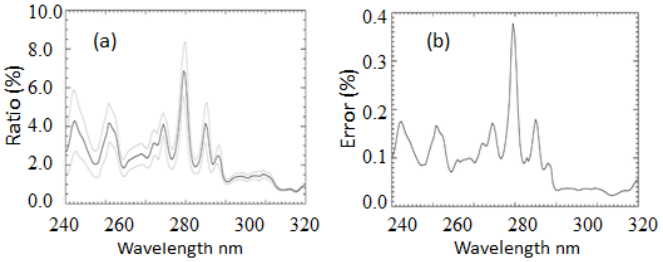


Fig 2. (a) Percent stray light contributions to signal during NOAA-20 NP Earth observation. (b) Albedo stray light calibration error for NOAA-20 NP.

## B. *System non-linearity*

NP flight software corrects nonlinearity for Earth observation prior to sending science raw data back to ground. The NP sensor specifies that the sensor nonlinearity shall not be larger than 2% and the nonlinearity calibration accuracy must be better than 0.2%. We modified the Suomi-NPP NP non-linearity calibration approach to reduce a quantization error at low radiance levels for the NOAA-20 NP. Long term trending of the sensor nonlinearity shows that in-flight nonlinearity of the sensors maintains less than 0.2%. The worst calibration error took place at the highest count level, about 30 counts out of 14600, i.e. 0.2% in absolute calibration. Fig. 3 (a) shows the calibration error over the entire signal dynamic range of the Suomi-NPP NP. Fig. 3 (b) tracks the stability of the maximum nonlinearity started from the first in-flight measurement for the Suomi-NPP NP. There are slightly lower values from the first six measurements made during the in-flight de-gassing phase. The NOAA-20 NP has a very similar performance: it has about 0.2% calibration error over the sensor dynamic level, and nonlinearity less than 0.25% since the launch [10]. The albedo error introduced by the system nonlinearity is the sum of squares of the calibration error, i.e., 0.023% for both the NPs.

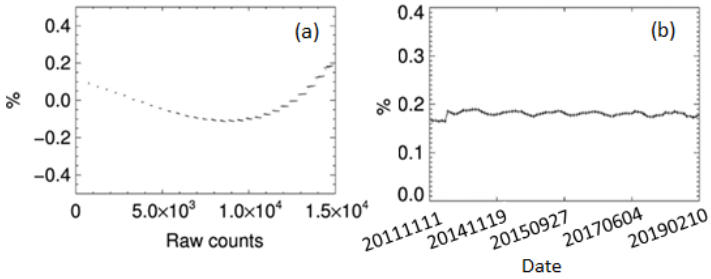


Fig 3. (a) Suomi-NPP nonlinearity calibration error over its entire

dynamic measurements. (b) Stability trending of the maximum nonlinear vs. sensor lifetime since NP launch.

### *C. Spectral Wavelength Calibration*

Calibration of the wavelength scale to 0.01 nm in accuracy effectively mitigates the wavelength-dependent albedo error. OMPS use a dichroic beam splitter to reflect most of the 250–310 nm light to the NP radiation spectrometer. Within the dichroic filter transition range, the sensor spectral response has the largest sensitivity to the wavelength variation, causing significant errors in radiometric calibration if the spectral wavelength remains uncorrected. Fig 4 shows the percent derivatives of the instrument radiometric response per nanometer shift over all spectral wavelengths. The wavelength of 305.7 nm has the maximum sensitivity of 28.76%/nm for the Suomi-NPP NP and 24.02%/nm for the NOAA-20 NP. With the calibration accuracy of a 0.01 nm wavelength, the absolute calibration error at 305.7 nm is about 0.29% for the Suomi NPP NP and 0.24% for the NOAA-20 NP.

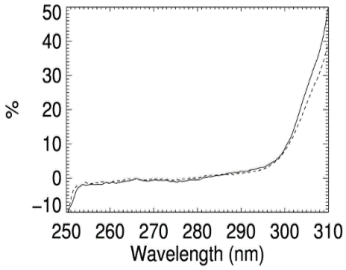


Fig 4. Percentage fractional derivatives per nm of the radiometric responses for the Suomi-NPP NP (solid) and the NOAA-20 NP (dashed). The data determines calibration errors caused by inaccurate wavelength knowledge.

The above sensitivity analysis of the NP in-flight data includes the impacts of all the wavelength-dependent quantities contained in Eq. 1, such as dark rate change and stray light distribution. Fig. 5 (a) shows a sensitivity relative to a 0.01 nm wavelength shift in absolute radiance calibration for the Suomi-NPP NP (solid line) and the NOAA-20 (dashed line). The average radiance error corresponding to a 0.01 wavelength shift is 0.22% and 0.26% for the Suomi-NPP NP and the NOAA-20, respectively; the maximum error is 0.67% and 0.88% for the Suomi-NPP NP and the NOAA-20, respectively.

In the dichroic region of 300 – 310 nm, the sensitivity is inconsistent with the observed solar measurements, thus introducing relatively large albedo errors. Fig 5 (b) shows the albedo sensitivity relative to a 0.01nm wavelength shift. For wavelengths less than 300 nm, the albedo error relative to a 0.01-nm wavelength shift is less than 0.05%. However, in the dichroic filter transition region, the errors suddenly increased to 0.3%, indicating that the radiance response within the dichroic spectral region is more sensitive than the solar irradiance response change under the same amount of spectral wavelength change in both NP sensors.

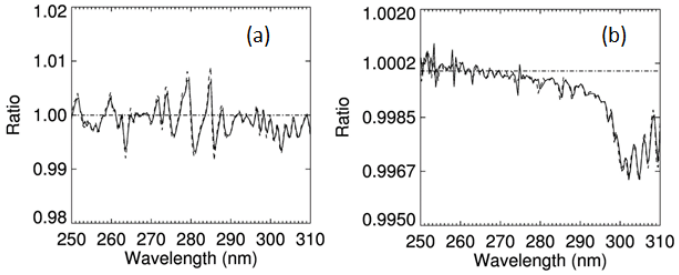


Fig 5. (a) Ratio of radiance change to a 0.01 nm wavelength shift for the Suomi-NPP NP (solid line) and the NOAA-20 (dashed line). (b) Ratio of albedo change to a 0.01 nm wavelength shift for the Suomi-NPP NP (solid line) and the NOAA-20 NP (dashed line).

### *D. Sensor temperature response*

One of the primary factors that causes NP in-flight response changes is attributed to wavelength variation due to the sensor thermal loading changes. Prelaunch calibration found NP wavelength shifted due to a flexing size of the NP instrument entry slit, and thus the throughput of the instrument. The sensitivity of sensor radiometric response to temperature was ~0.04% /°C for the Suomi-NPP NP and 0.06%/°C for the NOAA-20 NP. When transitioned from ground to orbit, the NP slit temperature changed by -22.5°C in the Suomi-NPP and -14.5°C in the NOAA-20 NP. Accordingly, NP spectral wavelength shifted around 0.09 – 0.13 nm in the Suomi-NPP and 0.11- 0.19 nm in the NOAA-20 NP.

In-flight sensor response change in accordance with wavelength variations is primarily attributed to short-term temporal (intra-orbit) variations as well as daily averaged long-term seasonal variations. A set of global observation data were used to extract wavelength change feature, including 1200 Earth view spectral images from the Suomi-NPP NP and 6000 Earth view spectral images from the NOAA-20 NP. Fig. 6 (a) shows an example of a short-term intra-orbit wavelength variation along the satellite track from the NOAA-20 NP. For the most of the observations, wavelengths vary less than ±0.01 nm, but for the observations made inside of the South Atlantic Anomaly (SAA) region as well as the two Polar Regions, are relatively large variation > 0.02 nm was observed. These regions have high-energy particles hitting the CCD detectors, causing significant noises in the sensor data. An error assessment of the intra-orbit wavelength change is addressed in the wavelength latitude dependency.

The seasonal sensor response changes are attributed primarily to a long-term seasonal wavelength fluctuation. Fig. 6 (b) shows an annual wavelength change is ±0.02 nm for the Suomi-NPP NP, ±0.01 nm for the NOAA-20 NP during sensor science observations. For an easy visualization and comparison, wavelength changes in the NOAA-20 NP were aligned with the Suomi-NPP NP data at the NOAA-20 NP first Earth measurement on January 10, 2018. A bi-weekly solar calibration mitigated the wavelength fluctuation to less than 0.01 nm for both the Suomi-NPP NP [7] and the NOAA-20 NP.

The maximum error in the absolute radiance calibration is 0.88% for the Suomi-NPP NP and 0.67% for the NOAA-20 NP. The average error in albedo calibration over all wavelength channels is 0.30% for both NP sensors.

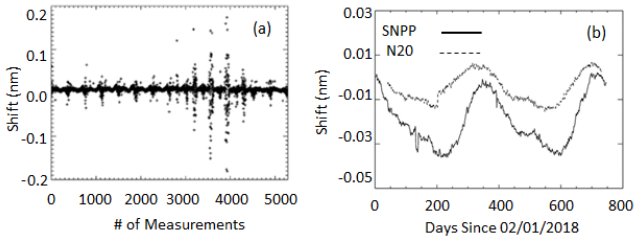


Fig 6. (a) Intra-orbit spectral wavelength variations from 14 orbit Earth radiance spectral data collected from the NOAA-20 NP. The NOAA-20 NP has a spatial resolution of 50 km x 50 km; it collects five times more spectral images than what the Suomi-NPP collects. (b) Seasonal wavelength fluctuations from the Suomi-NPP NP (lower solid line) and the NOAA-20 NP (upper dashed line).

The NP sensors present a latitude-dependent response change that contributes additional error to the SDRs. This is believed to stem from sensor thermal loading changes within an orbit, and wavelengths can shift by up to 0.015 nm. Fig. 7 shows a shift trend from 14-orbits wavelength change relative to a global average vs. latitudes. The maximum error in absolute calibration is 0.87% for the Suomi-NPP NP and 0.72% for the NOAA-20 NP. The albedo errors versus latitude are a function of wavelengths and can reach up to 0.45% in the wavelength region of 300 – 310 nm. The wavelength averaged albedo errors from daily global observations are less than 0.45 ± 0.006% (±1-σ standard deviation) for the Suomi-NPP NP (solid line), and less than 0.45 ± 0.1% (±1-σ standard deviation) for the NOAA-20 NP. Across-sensor comparison of the two NPs finds are relatively large discrepancy in radiance values can be 0.3 – 1.2 % along latitude when a relative wavelength difference between two NPs are greater than 0.01 nm.

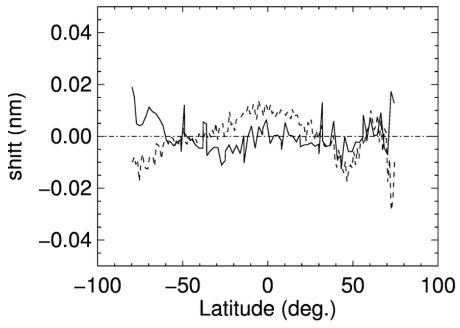


Fig 7. Relative wavelength variation to the average from 14 orbits vs. Earth view coordinate latitude for the Suomi-NPP NP (solid line) and the NOAA-20 NP (dashed line). The SAA region data was excluded in the figure.

### *E. Sensor noise*

Signal-to-noise ratio (SNR) is a precision term in radiometric calibration. We compute noise empirically as root-mean-square values from 2000 Earth view spectral images. Any broad-scale patterns caused by either wavelength variation or view condition were removed prior to the SNR calculation. Fig. 8 shows the wavelength dependent SNRs for the Suomi-NPP NP in Fig. 8 (a) and the NOAA-20 NP in Fig. 8 (b). The dashed lines are the requirements taken from the Table 2. The overall noise in the two NPs' science measurements meet the instrument requirements. However, the SAA region and the high-energy particles affect the NOAA-20 NP for wavelengths shorter than 256 nm, causing relative lower SNR.

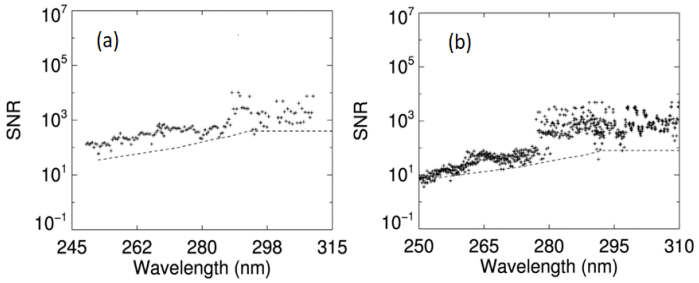


Fig 8. SNR from 14 orbit science measurement for (a) SNPP NP and (b) NOAA-20 NP. The data confidence level is 99.6% for Suomi-NPP, and 95% for NOAA-20. Each NP sensor meets its specification requirements as displayed by a dashed line.

### *F. Optical degradation*

Degradation of the NP sensors' optical system is common to radiance and irradiance measurements [11 and 12]. Fig. 9 shows an example of the Suomi-NPP instrument degradation trending along mission timeline for four ozone channels. A maximum of 3.5% degradation is observed at 250 nm, introducing about 2.75% error in the absolutely calibration of radiance and irradiance if no correction is made. The NOAA-20 NP currently has ~1% degradation since the launch.

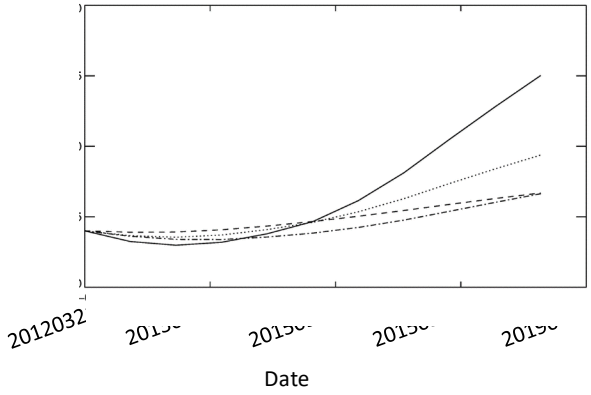


Fig. 9 An example of the Suomi-NPP NP degradation trending for four ozone wavelength channels.

### *G. Pixel Response Non-uniformity*

One of the SDR requirements states that the accuracy of the calibration at one pixel with respect to another pixel should be 1% or better. It is difficult to verify the requirement using in-flight data. In reality, this requirement verification was performed through a prelaunch lab test indirectly by using an integrating sphere that can produce a flat field. By examining the instability of the sphere radiance changes between two pixels' uniformity difference, the relative response accuracy was better than 0.7%.

### *H. Goniometry*

The response angular dependence of the on-board diffusers, known as goniometry, was measured in laboratory by using a synthetic solar illuminator at a variety of view angles that could cover in-flight observation conditions. Goniometry measurements of solar spectral irradiances can be used to correct the diffuser spectral and spatial features and removes undesirable diffuser small-scale irregularities. However, due to the difference of on-board instrument geometric angles from the lab observation angles, the goniometry calibration coefficients need to be linearly interpolated and/or extrapolated to fit the in-flight observation azimuth and elevation angles. According to our analysis against the laboratory measurements, the largest root mean squared (RMS) error in absolute irradiance was 0.38 for the Suomi-NPP NP and 0.29% for the NOAA-20 NP. Resultant albedo error is 0.15% for the Suomi-NPP NP and 0.11% for the NOAA-20 NP. Additionally, the impact of goniometric uncertainty is minimized by making the annual measurements with the reference diffuser at the same repeated solar angles.

## IV. ALBEDO CALIBRATION

Ozone retrievals require the accuracy no more than 2% in wavelength-independent albedo calibration. We used in-flight data to assess calibration errors over all wavelengths resulting from different SDR contributors. Assuming that errors from different contributors are uncorrelated, we calculate errors from the different contributors as a root mean square (RMS). Table 6 summarizes all averaged errors due to each of the SDR contributor. The absolute calibration error is about 2-3% for both NPs and the wavelength average albedo error is less than 2%. Due to lack of appropriate in-flight measurements, the verification of polarization was performed under laboratory condition. The polarization sensitivity in lab calibration was 2.4% to 2.8%, which contributed 0.05% error in absolute radiance calibration and0.27% in absolute irradiance calibration correspondingly. The wavelength independent error contributed 0.27% to the albedo accuracy.

The albedo error versus wavelengths was evaluated based on a comparison of measured normalized radiances (referred as NRs OBS) to calculated NRs (NRs-CAL) for specific measurement geometries, viewing conditions and climatological data. From a standard forward radiative transfer model TOMRAD [13 and 14], NRs were calculated for a given solar zenith and the relative azimuth, ozone concentration, surface pressure, and reflectivity. Results presented in Fig. 10 show that the wavelength-independent albedo error varies with wavelengths and meets the 2% requirement for all wavelengths except for the NOAA-20 NP short wavelengths where albedo accuracy was allowed to be increased to 3% for wavelengths between 250 and 260 nm.

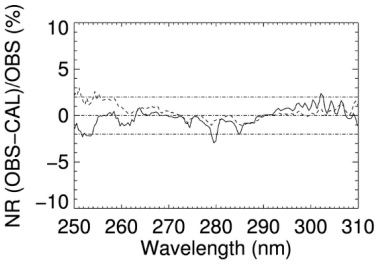


Fig 10. Albedo error estimates versus wavelength from a forward model calculation for the Suomi-NPP NP (solid line) and the NOAA-20 NP (dashed line).

TABLE 6
Summary of SDR attributors to the albedo error

| Sensor | NOAA20 NP/Suomi-NPP | | |
|---|---|---|---|
| Source of Error | Absolute Error (%) | | Albedo Error (%) |
| | Radiance | Irradiance | Albedo |
| Dark current | 0.34/0.53 | 0.003/0.007 | 0.03/0.05 |
| Smear | 0.02/0.02 | 0.02/0.02 | 0.03/0.03 |
| Electronic signal offset | 0.028/0.025 | 0.028/0.025 | 0.04/0.04 |
| Stray light | 0.75/0.78 | 0.75/0.78 | 0.38/0.38 |
| Linearity | 0.2/0.2 | 0.2/0.2 | 0.28/0.28 |
| Intra-orbit wavelength | 0.87/0.72 | 0.87/0.72 | 0.45/0.45 |
| Seasonal wavelength | 0.67/0.88 | 0.67/0.88 | 0.30/0.30 |
| Wavelength registraion | 0.67/0.88 | 0.67/0.88 | 0.30/0.30 |
| Sensor throughput change | 1.00/2.75 | 0.0/0.0 | 0.5/0.8 |
| Polarization | 0.05/0.05 | 0.27/0.27 | 0.27/0.27 |
| Goniometry | 0.0/0.0 | 0.29/0.38 | 0.11/0.15 |
| PRUN | 0.21/0.21 | 0.21/0.21 | 0.30/0.30 |
| RSS Total | 1.93/3.30 | 1.57/1.81 | 0.99/1.17 |
| Requirement | 8.00/8.00 | 7.00/7.00 | 2.00/2.00 |

## V. SUMMARY

The SDR performances of the Suomi NPP OMPS NP and the NOAA-20 OMPS NP both meet the SDR product requirements. The largest error term in the albedo calibration is the spectral wavelength calibration error, contributing about 60% to the overall error. On-orbit calibration of wavelength registration mitigated the wavelength errors to ~0.01 nm. Long-term seasonal wavelength fluctuations are corrected by the updates of the wavelength scale and solar calibration tables once every two-weeks. The two NP sensors' SDRs are very compatible from global representative observations; each senor has less than 2% error in earth albedo retrieval. Improvements in NOAA-20 NP calibration program have resulted in better performance than Suomi-NPP NP for major calibration requirements. Calibration of wavelength latitude dependency will be applied to the SDR algorithm in the future when necessary.

## ACKNOWLEDGMENT

The sensor data used in our analyses were generated at the S-NPP Interface Data Processing Segment and obtained from the NOAA Comprehensive Large Array-Data Stewardship System

and the JPSS Project GRAVITE System. The manuscript contents are solely the opinions of the authors and do not constitute a statement of policy, decision, or position on behalf of NOAA or the U.S. government. We also would like acknowledge NASA OMPS Science Investigator-led Processing Systems (SIPS) team for sharing calibration data to support our study.

## REFERENCES

[1] M. G. Dittman, E. Ramberg, M. Chrisp, J. V. Rodriguez, and A. L. Sparks et al., "Nadir ultraviolet imaging spectrometer for the NPOESS Ozone Mapping and Profiler Suite (OMPS)," in Proc. SPIE, 4814, Earth Observing Syst. VII, Sep. 25, 2002, p. 111, 10.1117/12.453748.

[2] M. Chrisp, J. V. Rodriguez, A. L. Sparks, N. H. Zaun, P. Hendershot, T. Dixon, R. H. Philbrick, and D. Wasinger, "Nadir Ultraviolet Imaging Spectrometer for the NPOESS Ozone Mapping and Profiler Suite (OMPS)", Proc. SPIE 4814, Earth Observing Systems VII, 111 (September 25, 2002); doi:10.1117/12.453748.

[3] C. Pan, M. Kowalewski, R. Buss, L. Flynn, X. Wu, M. Caponi, and F. Weng, Performance and Calibration of the Nadir Suomi-NPP Ozone Mapping Profiler Suite From Early-Orbit Images, IEEE Journal of Selected Topic in Applied Earth Observation and Remote Sensing. Volume 6, No. 3, June 2013.

[4] Donald F. Heath, Carlton L. Mateer, and Arlin J. Krueger, The Nimbus-4 Backscatter Ultraviolet (BUV) atmospheric ozone experiment — two years' operation. Pure and Applied Geophysics, 1973, Volume 106-108, Number 1, Page 1238.

[5] World Meteorological Organization, Global Ozone Research and Monitoring Project—Report No.52, http://ozone.unep.org/Assessment_Panels/SAP/Scientific_Assessment_2010/01-Contents_Preface.pdf .

[6] Joint Polar Satellite System (JPSS) Ground Project, NASA Goddard Space Flight Center, "OMPS Nadir Profiler Algorithm Theoretical Basis Document", https://www.star.nesdis.noaa.gov/jpss/documents/ATBD/D0001-M01-S01-005_JPSS_ATBD_OMPS-NP-Ozone_A.pdf , June 18, 2014.

[7] Matthew Kowalewski, Chunhui Pan, and Scott Janz, Early orbit operations performance of the Suomi NPP OMPS instrument, SPIE 8510, Earth Observing Systems XVII, 851007 (15 October 2012); doi: 10.1117/12.929753.

[8] Hong Grace Chen and Glen Jaross, SNPP OMPS Nadir Instruments Stray Light Corrections, http://www.star.nesdis.noaa.gov/star/documents/meetings/2014JPSSAnnual/dayTwo/04_Session4c_Chen_Stray_Light_Correction.pdf, STAR JPSS Annual Science Team Meeting, May 13, 2014.

[9] C. Pan , L. Zhou, C. Cao, L. Flynn, and E. Beach, Suomi-NPP OMPS Nadir Mapper's, Operational SDR Performance IEEE Transactions on Geoscience and Remote Sensing, VOL. 57, NO. 2, February 2019

[10] STAR OMPS SDR Team, NOAA-20 OMPS NP SDR Report (Validated Review Material), April 23, 2020.

[11] C. Pan; L. Flynn. Solar observation of Ozone Mapping and Profiler Suite nadir system during the first 3 years of on-orbit operation. J. Appl. Remote Sens. 9 (1), 094095 (August 21, 2015); doi:10.1117/1.JRS.9.094095.

[12] C. Pan, F. Weng, and L. Flynn, Spectral Performance and Calibration of the Suomi NPP OMPS Nadir Profiler Sensor, Earth and Space Science, Vol. 4, Issue 12, 26 DEC 2017, DOI: 10.1002/2017EA000336.

[13] Z. Cai et al., "Characterization and correction of global ozone monitoring experiment 2 ultraviolet measurements and application to ozone profile retrievals," J. Geophys. Res., Atmos., vol. 117, p. D07305, Apr. 2012, doi: 10.1029/2011JD017096.

[14] R. D. McPeters, G. J. Labow, and J. A. Logan, "Ozone climatological profiles for satellite retrieval algorithms," J. Geophys. Res., Atmos., vol. 112, p. D05308, Mar. 2007, doi: 10.1029/2005JD006823.